Communication—Electrochemical Reduction of N_2 to Ammonia by Vanadium Oxide Thin Films at Neutral pH: Oxophilicity and the NRR Reaction

Journal of The Electrochemical Society, 2021 **168** 026504
1945-7111/2021/168(2)/026504/4/$40.00

Communication—Electrochemical Reduction of N_2 to Ammonia by Vanadium Oxide Thin Films at Neutral pH: Oxophilicity and the NRR Reaction

Ashwin Ganesan,[=] Adaeze Osonkie,[=] Precious Chukwunenye, Ishika Rashed, Thomas R. Cundari,[z] Francis D'Souza,[*,z] and Jeffry A. Kelber[z]

Department of Chemistry, University of North Texas, Denton, Texas 76203-5017, United States of America

Electroreduction of N_2 to NH_3 is an energy- and environmentally-friendly alternative to the Haber-Bosch process. Little is known, however, about reactive sites for electrochemical nitrogen reduction reaction (NRR) at Earth-abundant oxide or oxynitride surfaces. Here, we report N-free $V^{III/IV}$-oxide films, created by O_2 plasma oxidation of polycrystalline vanadium, exhibiting N_2 reduction at neutral pH with an onset potential of −0.16 V vs Ag/AgCl. DFT calculations indicate that N_2 scission from O-supported V-centers is energetically favorable by ∼18 kcal mol^{-1} compared to N-supported sites. Theory and experiment yield fundamental insights concerning the effect of metal oxophilicity towards design of earth-abundant NRR electrocatalysts.
 [DOI: 10.1149/1945-7111/abde7f]

Manuscript submitted October 21, 2020; revised manuscript received January 7, 2021. Published February 2, 2021.

Although NH_3 production from N_2 and H_2 is critical for the world's food supply, the currently used Haber-Bosch process, run at high temperatures and pressures, accounts for as much as 2% of the world's energy consumption, and involves substantial production of CO_2. Much of this energy is supplied by fossil fuels.[1] Electrochemical NRR has emerged as a potential environmentally- and energy-friendly alternative to the Haber-Bosch process.[2,3] Indeed, recent studies of transition metal nitrides and oxynitrides[4–8] have shown promising results, but the nature of surface reaction sites and mechanisms remain to be understood. Isotope exchange mechanisms have identified a Mars-van Krevelen (MVK) mechanism for vanadium oxynitrides and chromium nitrides.[4,6] Pure VN, however, is inert towards NRR over a range of pH values.[9–12] Oxygen-free V-nitride nanoparticles and TiN films have also been reported as inactive towards NRR in acidic environments.[5] In contrast, Cr_2N has been reported as NRR active, while the oxynitride phase is inactive.[4] Taken together, these data suggest that metal oxophilicity plays an important role in oxynitride electrocatalytic behavior.

A specific vanadium oxynitride N site, with N1s binding energy of 396.5 eV, has been demonstrated to be NRR-related.[5] A similar observation was reported for Ti oxynitrides.[7] Very recent studies of such sites, generated by O_2 plasma oxidation of VN and vanadium oxynitride films,[13] indicate that such sites are not related to vanadium nitride/oxynitride bulk lattice sites in the rock salt structure, but are surface-specific sites associated with growth of a thin vanadium oxide overlayer, representing V≡N: or related unsaturated surface features on vanadium oxide. As discussed in a recent review,[14] such sites have been proposed to be key intermediates in NRR, suggesting that NRR actually occurs at O-supported vanadium Lewis acid sites. Mechanistically, NRR is a multi-proton coupled electron transfer process. Consequently, the catalyst surface size and ligand environment will impact the binding energy of the adsorbed N atoms and N_2 substrate, as well as the stability of reaction intermediates and hence the yields of ammonia product.

To obtain further insight into reactive Lewis acid centers for NRR, we focus on NRR of nitride-free V-oxide thin films formed by plasma oxidation of polycrystalline vanadium metal films. Ru- or Rh-supported ultrathin vanadium oxides—primarily thin V^{III} and V^{IV} oxides/hydroxides—are active heterogeneous catalysts for methanol oxidation.[15] Such vanadium oxides and hydroxides are electrochemically stable over a broad range of potentials and pH values.[16] Additionally, N-free, Au-supported Fe_3O_4 has recently been shown to be an active catalyst for electrochemical NRR.[9] N_2 absorption/reaction at O-supported Fe surface sites in Fe_3O_4 has also been observed at room temperature and ambient pressure by *operando* XPS,[17] further demonstrating that transition metal cationic sites on nitride-free oxide surfaces are important for NRR in some systems.

Herein, we present XPS and electrochemistry data indicating that nitride-free V oxides are active for NRR in neutral electrolyte. We also present DFT results demonstrating that O-supported V Lewis acid sites are active sites for NRR, and that such sites are energetically favorable for NRR reactions compared to corresponding N-supported vanadium sites, with similar conclusions for Ti sites, but not for Cr sites. These data prove that oxophilic transition metal oxides and surface-modified oxynitrides can be active for NRR, and that metal oxophilicity is a critical parameter in understanding the electrocatalytic behavior of oxides, oxynitrides and nitrides.

Experimental Methods

The vanadium film was deposited by magnetron sputter deposition (Meivac, Inc.) onto a commercially available fluorinated tin oxide (FTO) substrate at a substrate temperature of 675 K, using 4 mTorr Ar, 25 W for 7 min. The estimated film thickness based on manufacturer's information regarding deposition rates is ∼500 Å. Deposited films were transferred in ambient to a second vacuum system, described previously,[18] with separate chambers for plasma treatment and surface analysis. Briefly, the surface analysis chamber was equipped with a 140 mm mean radius hemispherical analyzer and an unmonochromatized dual anode X-ray source (Physical Electronics). XPS spectra were acquired at a constant analyzer pass energy (23.5 eV), except for survey scans (29.35 eV) with the analyzer aligned with the sample normal. XPS data analysis was carried out with commercially available software according to standard methods.[19] Conditions for O_2 plasma oxidation were 30 s of inductively coupled gas plasma treatment at 20 W and 40 mTorr O_2 pressure. This yielded an average V-oxide thickness of ∼13 Å. After plasma treatment, the sample was transferred to the UHV surface analysis chamber for XPS analysis. FWHM of $V2p_{3/2}$ are as follows: 1.3, 2, 2.7, 2.2, and 1.5 for V^0, V^{II}, V^{III}, V^{IV} and V^V, respectively.[20] Similarly, for deconvolution of O1s, a FWHM of 1.8 eV was used.[18] XPS binding energies were calibrated by referencing the oxide O1s signal to 530.2 eV.[20]

After XPS, the sample was transferred in air for electrochemical studies. Electrochemical measurements were carried out in a 3-electrode electrochemical cell in a 0.1 M Na_2SO_4 (pH = 7) electrolyte saturated with either Ar or N_2, using an EG&G PARSTAT Electrochemical Analyzer. The total concentration of nitrogen-containing compounds (mainly in the form of NO_3^- and NO_2^-) in the Na_2SO_4 supporting

[=]These authors contributed equally to this work.
*Electrochemical Society Fellow.
[z]E-mail: Thomas.Cundari@unt.edu; Francis.DSouza@UNT.edu; Jeffry.Kelber@unt.edu

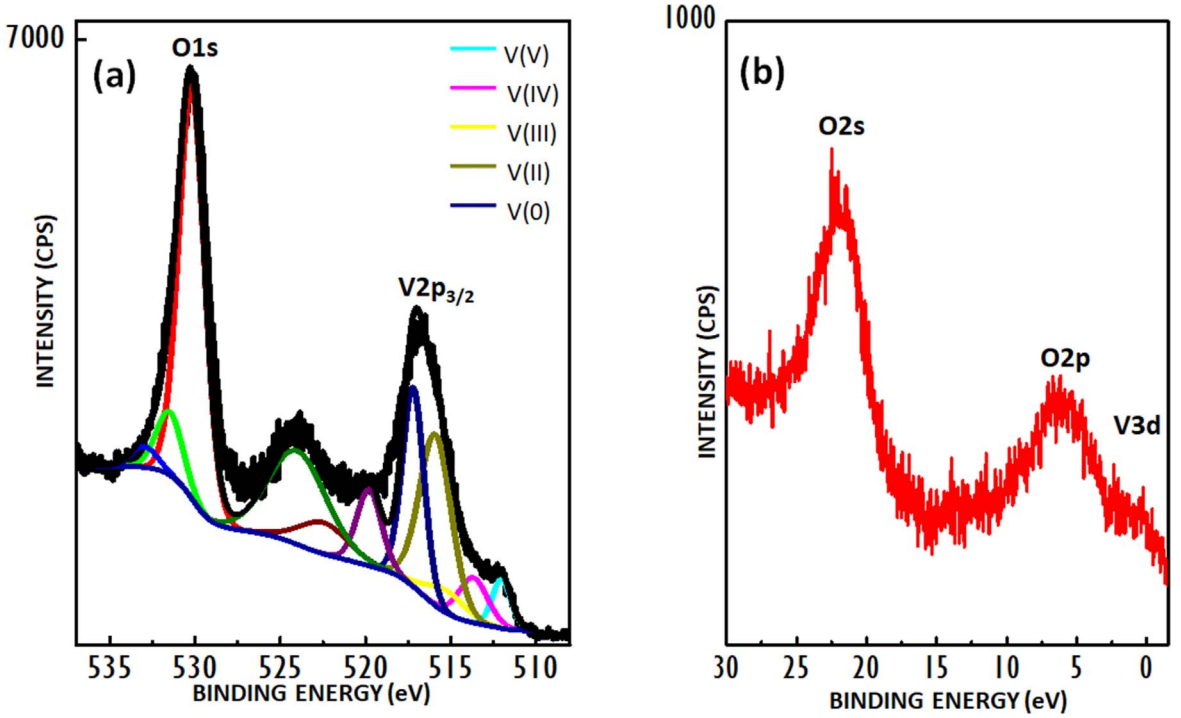

Figure 1. (a) XPS O1s and V2p core level spectra of a V film immediately after plasma treatment. Oxide components corresponding to various V oxidation state are from Ref. 17. (b) Corresponding valence band spectrum.

electrolyte (from Fischer Scientific) was ~4 ppm. A Ag/AgCl reference electrode and platinum wire counter electrode were used. Linear sweep voltammograms were recorded on the reductive side for the vanadium oxide film deposited onto FTO glass substrate. Control studies were also performed on plain conductive FTO glass as the working electrode. Multi-cyclic voltammograms (15 cycles) were recorded under the same electrochemical conditions to evaluate the robustness of the catalyst film.

For product analysis, a 2 cm^2 V/VO_x coated FTO electrode was dipped in 20 ml of 0.1 M sodium sulphate under N_2 atmosphere. Electrolysis was performed at an applied potential of −0.80 V vs Ag/AgCl for 1.5 h. Next, a 10 ml sample of the electrolysis solution was treated with 0.5 ml of 0.55 M NaOH containing 5 wt% salicyclic acid and sodium citrate, 100 μl of sodium nitroprusside dehydrate and 100 μl of sodium hypochlorite to generate indophenol blue from the ammonia formed during the bulk hydrolysis experiment.[3,7] After maintaining the solution at room temperature for 30 min, the absorbance of the solution was measured using a JASCO V-670 spectrophotometer. A control experiment using commercial ammonia to produce indophenol blue using the above procedure was also performed. In both the cases, the produced indophenol blue revealed similar spectral characteristics.

All computations were performed using the VASP package (version 5.4.4).[21] All simulations were spin polarized, and implemented PAW and projector augmented wave methods. Calculations utilized a plane wave cutoff energy of 500 eV; SCF convergence was considered to be $<1 \times 10^{-5}$ eV. Surface calculations, done in an asymmetrical unit cell of ~8.1 × 8.1 × 28.8 Å, used a K-point mesh of 3 × 3 × 1.[22] Calculations utilized the Methfessel–Paxton method[23] with $\sigma = 0.2$ eV.

Results and Discussion

XPS O1s and V2p core level spectra of the V-oxide sample after plasma oxidation but prior to air exposure or electrochemistry are shown in Fig. 1a, with the corresponding valence band spectrum (Fig. 1b). The corresponding survey scan (not shown) exhibited no Sn- or F-related XPS or Auger features, consistent with a pinhole free film ~500 Å thick. No N 1 s signal was observed in the initial V-oxide sample. The $V2p_{3/2}$ spectrum exhibits both a metallic V feature at 513 eV binding energy, and a feature near 515 eV, indicative of a V^{III} oxidation state.[20] The width of this feature indicates the presence of V^{IV} oxide, as well as less intense components corresponding to higher V oxidation states.[15,20] The O1s spectrum exhibits a main feature near 530 eV, consistent with the lattice O of a V-oxide, with a smaller higher binding energy indicative of surface hydroxylation.[20] Assuming a stoichiometry of V_2O_3, the O1s, V-oxide and V metal spectra indicate an average V-oxide thickness of ~13 Å, prior to air exposure or electrochemical testing. The valence band spectrum (Fig. 1b) exhibits significant electron density at the Fermi level, consistent with a thin oxide overlayer on vanadium metal substrate.

Upon immersion in solution, the V/VO_x film-coated FTO sample exhibited current-voltage and cyclic voltammetry behaviors as shown in Figs. 2a and 2b, respectively. Current-voltage curves show increased cathodic current in N_2-saturated solution as compared to Ar-saturated solution, indicating NRR activity. Uncoated FTO samples exhibited negligible activity. Repeated cyclic voltammetry (CV) studies indicate that this behavior is fairly stable under experimental conditions, although with a slight increase in cathodic current upon increased cycling. During anodic excursion of the potential, a new irreversible wave at −0.15 V was observed. This feature was also present in Ar-saturated multi-CV experiments suggesting that it is likely due to re-oxidation of vanadium sites. The data in Fig. 2a demonstrate that the vanadium oxide thin film is reactive towards N_2 at cathodic conditions, even at pH 7. The similar cathodic current behaviors in Ar− and N_2− saturated solution (Fig. 2a) indicate that the vanadium oxide electrode supports both the hydrogen evolution reaction (HER) and NRR, though with a slightly retarded onset potential (−0.16 V vs Ag/AgCl) for NRR. The slight increase in cathodic current, at potentials more negative than ~−1.0 V vs Ag/AgCl, upon repeated cycling (Fig. 2b), is also consistent with a slow but monotonic increase in the thickness of the oxide/hydroxide surface layer.[15]

Next, bulk electrolysis was performed in the presence of N_2 (see Experimental Methods for details), and the bulk-produced ammonia was used to generate indophenol blue whose spectrum is shown in

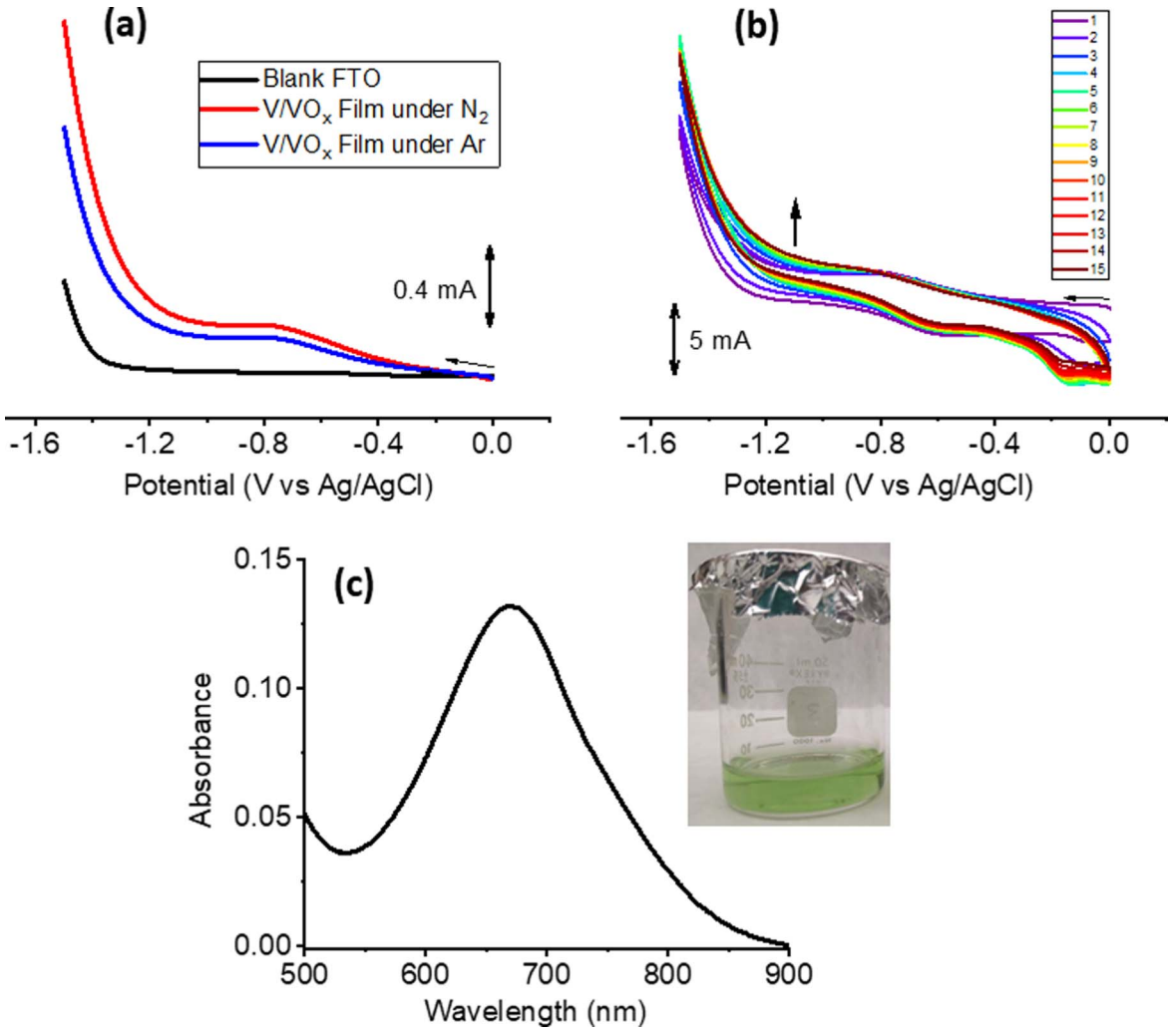

Figure 2. (a) Linear scan current-voltage curves for (black) a blank FTO sample, (blue) the vanadium oxide film in Ar-saturated solution and (red) in N_2 –saturated solution. (b) multiple cyclic voltammograms of vanadium oxide film in N_2–saturated solution. The arrow marks the trend in cathodic current levels with repeated cycling. Scan rate = 100 mV s^{-1}. Solution conditions: 0.1 M Na_2SO_4 at pH = 7. (c) Absorption spectrum of indophenol blue generated from ammonia produced by bulk electrolysis (see Experimental Methods for details). Figure inset: picture showing solution color of the produced indophenol blue.

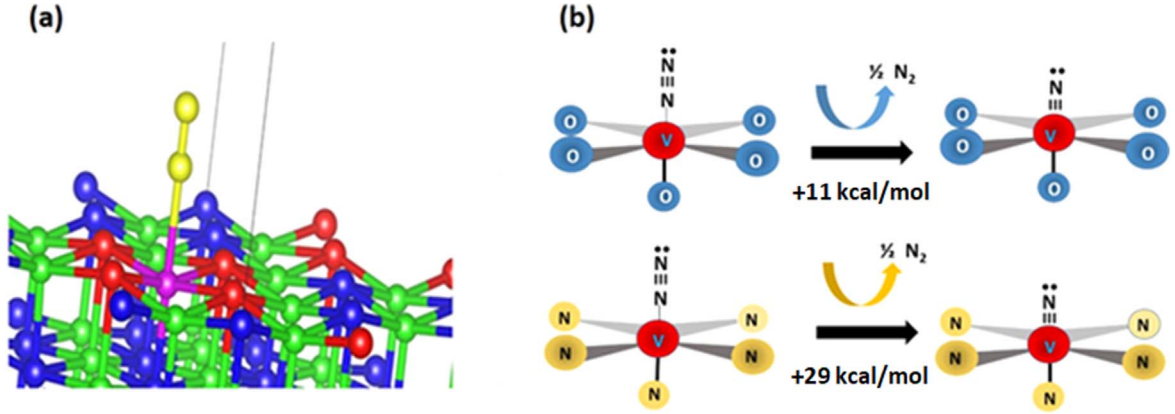

Figure 3. (a) Portion of DFT-optimized surface unit cell for $[V]_O$-N_2 model. Colors: V to which N_2 is coordinated = magenta; other V = green; nitrogen atoms of N_2 = yellow; other N = blue; surface O = red. In $[V]_N$-N_2 model, surface O are replaced with N then re-optimized. From these were generated $[V]_{N,O}$=N: models by removal of the terminal N of N_2, and $[V]_{N,O}$ models by removal of both nitrogen atoms of N_2. After each change to the surface, the model was re-optimized with DFT methods as described in Experimental Methods. (b) Computational results showing reaction energetics N_2 scission on O-supported V surface sites are substantially lower than on N-supported sites.

Fig. 2c. A broad band with maxima at 670 nm was observed that agreed well with the commercial dye at this pH. Using the optical density and molar extinction coefficient value of 2.5×10^5 $M^{-1}cm^{-1}$, the measured concentration of indophenol blue (= $[NH_3]$) was found to be 5.28×10^{-7} M, revealing appreciable efficiency. Importantly, similar experiments carried out in Ar-saturated solution in the absence

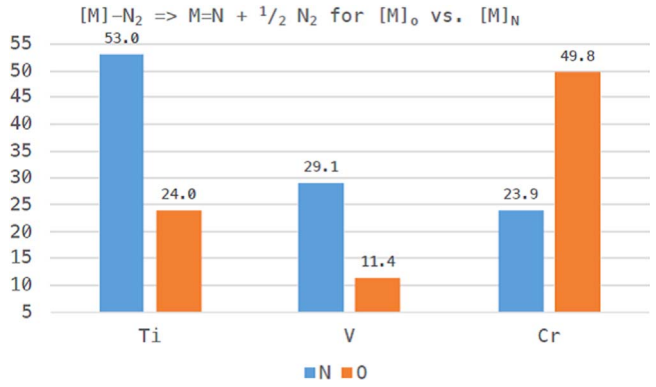

Figure 4. Energetics (in kcal mol^{-1}) for N_2 scission on metal-oxynitide surface sites ([M]–N_2) → [M]≡N: + ½ N_2, for M = Ti, V and Cr.

of N_2 showed no evidence of NH_3. Therefore, formation of NH_3 as one of the products of catalytic reduction of nitrogen by the V/VO_x film electrode was confirmed. Further, additional control experiments were performed to verify whether inorganic contaminants like NO_3^- and NO_2^- (present in trace quantities in the Na_2SO_4 supporting electrolyte) would produce NH_3. For this, independent bulk electrolysis experiments were performed using freshly made vanadium oxide film electrodes in the presence of 5×10^{-7} M KNO_3 in Ar saturated solution, and in the presence of 1×10^{-7} M $NaNO_2$ in Ar saturated solution. Such experiments produced no measurable amounts of NH_3, ensuring that the reported NRR activity is indeed due to N_2 electroreduction and not from nitrogen-containing contaminants present in the supporting electrolyte.

DFT calculations were carried out to determine the change in energy for the reaction

$$[V] - N_2 \rightarrow [V] \equiv N: \ + 1/2N_2 \qquad [1]$$

for a surface V coordinated to 4 surface oxygens, $[V]_O$ model—modeling an unsaturated V surface site in a V-oxide.[24] Such a reaction pathway mimics the proposed initial, activating step in the NRR process.[14] Similar calculations were then carried out for a corresponding models for the N_2 activation reaction at a corresponding V center bonded to 4 surface N neighbors, $[V]_N$, as a model of a N-rich, rock salt-structured VN surface; these models (Fig. 3a) were validated in earlier experimental-theoretical studies of V-oxynitrides.[13] As expected, bonding of N_2 to a surface V was weak for both models, $\Delta E_{bind}(N_2) = -3$ kcal mol^{-1} for $[V]_O$ and +1 kcal mol^{-1} for $[V]_N$. N_2 scission is calculated to be more endothermic by 18 kcal mol^{-1} ($\Delta E_{scission} = +29$ vs +11 kcal mol^{-1}) at the $[V]_N$ vs $[V]_O$ site, Fig. 3b. Previous experiments and calculations indicate that creating O vacancies is more facile than creating N vacancies for V-oxynitride materials.[13] These results are bolstered by experiments indicating that vanadium nitride and oxynitride surfaces are activated for NRR by a specific N 1 s surface state at 396.5 eV adjacent to a V oxide site.[5,6] Taken together, these data infer that V-oxynitrides that are O-rich are superior NRR electrocatalysts due to greater access to unsaturated $[V]_o$≡N: entities.

Extension of the above calculations to corresponding Ti and Cr-based systems is shown in Fig. 4. The data show that for oxophilic Ti and V, the energetics of N_2 dissociation are more favorable at O-supported rather than N-supported metal cation centers, provide an explanation why oxynitride phases—or, possibly, oxynitrides with thin oxide overlayers[10]—are NRR active. In contrast, the data in Fig. 4 indicate that the energetics are reversed for Cr, indicating more favorable energetics for N_2 dissociation at chromium nitride sites, consistent with experiment.[4] Further experimental and theoretical studies to unravel the mechanistic details of stepwise proton addition to the $[V]_o$≡N: site to produce NH_3 are in progress in our laboratories.

Conclusions

Photoemission and electrochemistry data indicate that vanadium oxide thin films, produced by O_2 plasma oxidation of V metal, are NRR active in pH 7 solution. These data are in agreement with DFT calculations indicating that the scission of N_2 at O-supported V centers is energetically more favorable than at corresponding N-supported centers by 18 kcal mo^{-1}. DFT calculations indicate that N_2 dissociation is also favored at O-supported Ti centers to an even greater degree (29 kcal mol^{-1}), but that this situation is reversed for Cr, consistent with experimental data regarding the NRR activities and inactivities of Ti, V or Cr oxide/oxynitride or nitride phases. These data therefore demonstrate that N-free V oxides are active for NRR, and that the recently-quantified concept of metal oxophilicity[25] is a central and predictive factor for the design of effective NRR electrocatalysts.

Acknowledgments

T.R.C. thanks the National Science Foundation for partial support of this research through grant CHE-1953547, and their support of the UNT CASCaM HPC cluster via Grant CHE-1531468. Partial support was also provided by UNT through internal funding through the Office of the Vice President for Research and the College of Science, and is gratefully acknowledged. Dr. Slavomir Nemsak (LBNL) is also acknowledged for stimulating discussions.

ORCID

Francis D'Souza https://orcid.org/0000-0003-3815-8949

References

1. S. Licht, B. Cui, B. Wang, F.-F. Li, J. Lau, and S. Liu, *Science*, **345**, 637 (2014).
2. K. Kim, N. Lee, C. Yoo, J. Kim, H. C. Yoon, and J. Han, *J. Electrochem. Soc.*, **163**, F610 (2016).
3. G. Qing, R. Ghazfar, S. T. Jackowski, F. Habibzadeh, M. M. Ashtiani, C. Chen, M. R. Smith, and T. W. Hamann, *Chem. Rev.*, **120**, 5437 (2020).
4. J. Nash, X. Yang, J. Anibal, M. Dunwell, S. Yao, K. Attenkofer, J. G. Chen, Y. Yan, and B. Xu, *J. Phys. Chem. C*, **123**, 23967 (2019).
5. X. Yang, J. Nash, J. Anibal, M. Dunwell, S. Kattel, E. Stavitski, K. Attenkofer, J. G. Chen, Y. Yan, and B. Xu, *J. Am. Chem. Soc.*, **140**, 13387 (2018).
6. X. Yang, S. Kattel, J. Nash, X. Chang, J. H. Lee, Y. Yan, J. G. Chen, and B. Xu, *Angew. Chem. Int. Ed.*, **131**, 13906 (2019).
7. S. Kang, J. Wang, S. Zhang, C. Zhao, G. Wang, W. Cai, and H. Zhang, *Electrochem. Commun.*, **100**, 90 (2019).
8. J. Zhang, Y. Ji, P. Wang, Q. Shao, Y. Li, and X. Huang, *Adv. Funct. Mater.*, **30**, 1906579 (2020).
9. H. Du, T. R. Gengenbach, R. Hodgetts, D. R. MacFarlane, and A. N. Simonov, *ACS Sustain. Chem. Eng.*, **7**, 6839 (2019).
10. R. Y. Hodgetts, A. S. Kiryutin, P. Nichols, H.-L. Du, J. M. Bakker, D. R. Macfarlane, and A. N. Simonov, *ACS Energy Lett.*, **5**, 736 (2020).
11. J. Choi, H.-L. Du, C. K. Nguyen, B. H. R. Suryanto, A. N. Simonov, and D. R. MacFarlane, *ACS Energy Lett.*, **5**, 2095 (2020).
12. J. Choi, B. H. R. Suryanto, D. Wang, H.-L. Du, R. Y. Hodgetts, F. M. F. Lallana, D. R. MacFarlane, and A. N. Simonov, *Nature Commun.*, **11**, 5546 (2020).
13. A. Osonkie, V. Lee, P. Chukwunenye, T. Cundari, and J. A. Kelber, *J. Chem. Phys.*, **153**, 144709 (2020).
14. J. Hou, M. Yang, and J. Zhang, *Nanoscale*, **12**, 6900 (2020).
15. B. von Boehn and R. Imbihl, *Front. Chem.*, **8**, 707 (2020).
16. M. Privman and T. Hepel, *J. Electroanal. Chem.*, **382**, 137 (1995).
17. G. D. Degaga, M. Trought, S. Nemsak, E. J. Crumlin, M. Seel, R. Pandey, and K. A. Perrine, *J. Chem. Phys.*, **152**, 54717 (2020).
18. B. Dong, A. Oyelade, N. Nandagopal, and J. A. Kelber, *Surf. Coat. Technol.*, **314**, 45 (2017).
19. D. Briggs and M. P. Seah, *Practical Surface Analysis*, Second edition, Auger and X-ray photoelectron spectroscopy, **1**, 657 (1990).
20. M. C. Biesinger, L. W. M. Lau, A. R. Gerson, and R. S. C. Smart, *Appl. Surf. Sci.*, **257**, 887 (2010).
21. J. Häfner and G. Kresse, "The vienna ab-initio simulation program VASP:An efficient and versatile tool for studying the structural, dynamic, and electronic properties of materials." *Properties of Complex Inorganic Solids*, ed. A. Gonis, A. Meike, and P. E. A. Turchi (Springer, Berlin: NY) (1997).
22. H. J. Monkhorst and J. D. Pack, *Phys. Rev. B*, **13**, 5188 (1976).
23. M. Methfessel and A. Paxton, *Phys. Rev. B*, **40**, 3616 (1989).
24. W. Bao, C. Broholm, G. Aeppli, S. A. Carter, P. Dai, T. F. Rosenbaum, J. M. Honig, P. Metcalf, and S. F. Trevino, *Phys. Rev. B*, **58**, 12727 (1998).
25. K. A. Moltved and K. P. Kepp, *J. Phys. Chem. C*, **123**, 18432 (2019).